IEEE Access
Multidisciplinary ⋮ Rapid Review ⋮ Open Access Journal

Received 15 August 2025, accepted 22 September 2025, date of publication 29 September 2025, date of current version 3 October 2025.

Digital Object Identifier 10.1109/ACCESS.2025.3615553

RESEARCH ARTICLE

Detection of Nonstationary Events in Motor Signals Using Nonparametric Statistical Hypothesis Testing

EDUARDO VAZ FAGUNDES RECH[1,2], LEVY ELY DE LACERDA DE OLIVEIRA[2], AND WILSON CESAR SANT'ANA[1,3], (Senior Member, IEEE)

[1]Office of Research and Graduate Studies (PRPPG—PPGEEL), Federal University of Itajubá (UNIFEI), Itajubá 37500-903, Brazil
[2]Research and Development Department, Gnarus Institute, Itajubá 37502-485, Brazil
[3]Institute of Systems Engineering and Information Technology (IESTI), UNIFEI, Itajubá 37500-903, Brazil

Corresponding author: Wilson Cesar Sant'Ana (wilson_santana@ieee.org)

The Article Processing Charge (APC) for the publication of this research was funded by the Coordination for the Improvement of Higher Education Personnel (CAPES) (ROR ID: 00x0ma614). For open access purposes, the authors have assigned the Creative Commons CC BY license to any accepted version of the manuscript.

ABSTRACT This work presents a lightweight statistical method for detecting nonstationarities in motor current signals, aiming to improve the diagnosis of transient events such as sudden load changes or inverter disturbances. Unlike traditional MCSA techniques that rely on spectral analysis, the proposed framework segments the signals into non-overlapping windows and extracts global statistical features to capture distributional changes over time. These features are compared using nonparametric hypothesis tests with p-value fusion strategies, enhancing robustness, with an adaptive buffering scheme based on Wasserstein distance to allow the system to adjust to signal variability. Results indicates accuracy reaches values as high as 95.9% with the false positive and false negative rates go as low as 7.7% and 0% respectively for both Monte Carlo simulations and real-world tests (from 529 MCSA signals), demonstrating strong potential for real-time, embedded, and scalable motor health monitoring without requiring complex signal decomposition or machine learning models.

INDEX TERMS Adaptive buffer, condition monitoring, hypothesis testing, induction motors, motor current signature analysis (MCSA), Monte Carlo simulation, nonstationary detection, predictive maintenance, P-value fusion, Wasserstein distance.

I. INTRODUCTION

Monitoring and diagnosing the condition of electric motors is essential to ensuring the reliability and operational continuity of industrial processes. Electric motor faults can lead to costly downtime, damage to equipment, and safety hazards [1]. Among various monitoring techniques, Electrical Signature Analysis (ESA), particularly Motor Current Signature Analysis (MCSA), has gained prominence due to its noninvasive nature and ability to detect a wide range of faults such as broken bars, eccentricity, and winding short-circuits [2].

However, traditional MCSA techniques often rely on frequency domain tools like the Fourier Transform, which assumes the signal is stationary [3]. This assumption implies that the statistical characteristics of the signal - such as its mean, variance and higher-order moments - remain constant over time [4]. In reality, motor signals are often nonstationary due to mechanical load changes, power supply fluctuations, or system transients.

These nonstationarities present a fundamental challenge to spectral methods, resulting in distorted spectral representations such as frequency leakage, side lobes, and ambiguous harmonic content. This issue leads to reduced sensitivity and accuracy in fault detection [3].

Recent MCSA-based fault detection methods for induction motors have explored advanced signal processing and intelligent classification techniques. Garcia-Bracamonte et al. combined Independent Component Analysis and Neural

The associate editor coordinating the review of this manuscript and approving it for publication was Pinjia Zhang.

Networks for broken bar detection, achieving high accuracy but relying on a handcrafted spectral segmentation [5]. Song et al. used CEEMDAN to enhance bearing fault visibility in stator currents, though the method is still sensitive to noise and requires manual IMF selection [6]. Zamudio-Ramirez et al. proposed a novel approach using stray flux signals and dimensionality reduction for detecting gearbox wear, but it requires additional sensors not typically available in standard motor setups [7]. Yelpale et al. developed a fuzzy decision system to switch between FTT and Wavelet analysis based on motor load and signal behaviour, improving efficiency but dependent on accurate fuzzy rules [8]. Liu et al. introduced a beam-forming-based spectrum method robust to varying loads and noise, but it adds computational complexity and parameter sensitivity [9]. Li et al. proposed a generalized auto-correlation function method with a embedded period estimation to detect bearing faults under varying-speed working conditions, but requires order-tracking methods which needs extra instruments that may be unavailable and inconvinient to be installed in some machineries [10]. All these methods aim to create a robust diagnosis nonstationary MCSA signals at the cost of computational complexity, sensitivity, and poor generalization for different operation conditions, which is especially bad if the input is a stationary MCSA signal.

In the nonstationarity detection front, Souza et al. used EMD to estimate the trend of the signal and time-frequency analysis to the evolution in the local energy of the signal, but with the major drawback of only detecting trend nonstationarities [11]. Chu and Mak employed a time-varying linear model with parameters estimated with a weighted maximum a posteriori estimator state-regularized via a QR decomposition-based RLS, at the cost of computational complexity for parameter estimation [12]. Amoud et al. employed a time-frequency kernel SVM with a set of generated surrogate signals to train the stationary class of the algorithm, but it greatly depends on a the set of surrogate signals for good detection accuracy [13]. Zhu et al. proposed two ways to detect nonstationary covariance matrices, the first uses a Generalized Likelihood Ratio test with high computational cost, and the second using the Rao test which have a lower cost compared to the first but has a lower accuracy [14]. Khadidja et al. employed a Kalman Filter modeled by a Time-Varying AutoRegressive model with thresholding detection to detect Epileptic Spikes, since it was made to detect nonstationary triangular spikes, it suffers from poor generalization of nonstationarity detection [15]. Sun et al. used Cointegration Analysis based LASSO to effectively describe and model the relation among the nonstationary variables in a process, however it requires knowledge of which process variables are nonstationary to create an effective model [16]. Tian et al. perform EEMD to decompose vibration signals into IMFs and separate them into stationary and nonstationary components via the Augmented Dickey-Fuller test, at the cost of complexity due to the ensemble decomposition [17]. Ozkan et al. proposed using a Markov model with Neyman-Pearson characterization for a highly efficient with tunable false alarm rate, but requires model training for it be able to detect a type of nonstationary event [18]. All this methods aims to detect nonstationary events on time series and either classify it and nonstationary or separate its components from the stationary part of the data, but they suffer from high computational cost, highly nonstationary shape detection speciality, making them bad at detecting other type of events them from their design, or external knowledge or tools that might not be available in a industrial process.

Contrary to that aim, the objective of this work is to develop a statistical framework to robustly detect nonstationary behavior in motor current signals by directly analyzing changes in the statistical distributions of signal features over time. The proposed method is designed to be computationally lightweight, interpretable, and effective for real-time development in industrial systems. Instead of relying on deep learning or complex decompositions, it leverages classical hypothesis testing and p-value fusion to identify significant deviations from normal behaviour.

This paper is organized as follows: section II theoretical (statistical) concepts required to further develop the proposition; section III presents the procedure applied to extract features from signals and detection of nonstationarity; section section IV presents the results obtained either from simulation and from real-world motor current signals; section section V concludes the paper and proposes future work.

II. THEORETICAL CONCEPTS

This section presents the theoretical concepts of the techniques employed in this work for nonstationarity detection in motor current signals. It covers core statistical tools, signal representation techniques, and the reasoning behind the detection strategies used.

A. STATIONARITY AND NONSTATIONARITY IN TIME-SERIES

A stationary signal is one whose statistical properties (such as mean, variance, and higher-order moments) do not change over time. In contrast, nonstationary signals exhibit time-varying statistical behaviour, often due to changes in system dynamics or external disturbances [4]. In the context of induction motors, these nonstationarities may arise due to load variations, transient faults, or switching disturbances from the grid or power electronics [1].

Detecting these deviations is crucial, as they often precede more significant failures or performance degradation. Traditional spectral techniques (such as FFT) assume signal stationarity and can be ineffective in capturing such changes, especially when the events are transient, localised, or masked by noise.

B. WASSERSTEIN DISTANCE

The Wasserstein distance, also known as the Earth Mover's Distance, is a measure of dissimilarity between two probability distributions that accounts for both magnitude of the difference and the location of the probability mass. Intuitively, it reflects the minimal "cost" of transforming one distribution into the other, where cost is defined in terms of the "amount" of distribution shifted times the "distance" it is moved - much like the effort required to move piles of earth (hence the name Earth Mover's Distance) [19], [20]. Let μ and ν be two probability measures over a metric space $\chi \subseteq \mathbb{R}^d$. The p-Wasserstein distance of order $p \geq 1$ between them is defined as:

$$W_p(\mu, \nu) = \left(\inf_{\gamma \in \Gamma(\mu,\nu)} \int_{\chi \times \chi} ||x - y||^p d\gamma(x, y)\right)^{\frac{1}{p}} \quad (1)$$

where $\Gamma(\mu, \nu)$ is the set of all joint distributions $\gamma(x, y)$ whose marginals are μ and ν and $||\cdot||$ represents the metric over that space [20].

For one-dimensional distributions, the Wasserstein distance has a closed-form and more efficient expression. Let F(t) and G(t) be the cumulative distribution functions of μ and ν, respectively; then:

$$\begin{aligned} W_p(\mu, \nu) &= \left(\int_{-\infty}^{\infty} |F(t) - G(t)|^p dt\right)^{\frac{1}{p}} \\ &= \int_0^1 |F^{-1}(t) - G^{-1}(t)|^p dt)^{\frac{1}{p}} \end{aligned} \quad (2)$$

This metric is uniquely suitable for detecting distributional drift in time-series because it is sensitive to gradual or cumulative changes, which often occur during transient processes in motor signals and, unlike Kullback-Leibler (KL) divergence or other entropy-based metric, it does not require density estimation or support overlap [19].

C. NONPARAMETRIC HYPOTHESIS TESTING FOR DISTRIBUTIONAL CHANGE

In the context of nonstationarity detection, hypothesis testing serves as a formal statistical approach to determine whether two samples originate from the same underlying distribution. In this project, we apply nonparametric two-sample tests, which do not assume any particular shape for the distributions being compared. These tests were chosen because they are robust and applicable to real-world signal data, where distributional assumptions often do not hold. We focus on three widely used tests: Anderson-Darling, Kolmogorov-Smirnov, and Cramér-von Mises.

1) ANDERSON-DARLING TEST (AD)

The Anderson-Darling 2-sample test is an extension of the original AD test, which is used to compare a sample to a known distribution. In the two-sample version, it evaluates whether two samples come from the same underlying distribution by comparing their cumulative distribution functions (CDFs) [21], [22] [23].

Mathematically, the test is based on a measure of the weighted squared difference between the empirical cumulative distributions of the samples. The AD statistic gives more weight to differences in the tails of the distribution, making it especially sensitive to outliers or heavy-tailed deviations [21], [22]. It can be defined has:

$$AD^2 = \frac{nm}{n+m} \int_{-\infty}^{\infty} \frac{(F_n(x) - G_m(x))^2}{H_N(x)(1 - H_N(x))} dH_N(x) \quad (3)$$

where $F_n(x)$ is the empirical distribution of the first set with n samples, $G_m(x)$ is the empirical distribution of the second set with m samples and $H_N(x) = \frac{nF_n(x)+mG_m(x)}{n+m}$ is an weighted average empirical distribution of the two sets.

2) KOLMOGOROV-SMIRNOV TEST (KS)

The Kolmogorov-Smirnov 2-sample test measures the maximum absolute difference between the empirical cumulative distribution functions of two samples:

$$D = \sup_x |F_n(x) - G_m(x)| \quad (4)$$

where F_n and G_m are the empirical CDFs of the samples of size n and m. This test is nonparametric and sensitive to general differences in distribution, including location and shape, though it is more attuned to differences near the center of the distributions [24], [25].

The KS test has the advantage of being computationally efficient, and its exact distribution under the null hypothesis is well-studied, allowing for analytical p-value computation [24], [25].

3) CRAMÉR-VON MISES TEST (CvM)

The Cramér-von Mises 2-sample test is closely related to the KS test, but instead of focusing on the maximum deviation, it considers the integrated squared difference between the empirical CDFs [25], [26]:

$$\omega^2 = \frac{nm}{n+m} \int_{-\infty}^{\infty} (F_n(x) - G_m(x))^2 dH(x) \quad (5)$$

where $H_N(x) = \frac{nF_n(x)+mG_m(x)}{n+m}$

This test is often considered a compromise between KS and AD tests, being sensitive to both central and peripheral differences in distributions, but less affected by outliers than AD.

D. P-VALUE FUSION STRATEGIES

When multiple hypothesis tests are performed in parallel it becomes necessary to combine their p-values into a single scalar decision metric. This is especially important to reduce Type I errors (false positives) from multiple testing and to arrive at a coherent test statistic for classification. We explore two methods for this fusion: Fisher's method and the Harmonic Mean P-value.

1) FISHER'S METHOD FOR COMBINING P-VALUES

Fisher's Method is a likelihood-ratio-based technique for combining independent p-values. If $p_1, p_2, \ldots, p_k$ are p-values from k independent tests, the Fisher statistic is:

$$X^2 = -2\sum_{i=1}^{k} ln(p_i) \tag{6}$$

Under the null hypothesis (that all tests are true), X^2 follows a chi-squared distribution with 2k degrees of freedom, which yields a valid test for combined evidence against the null [27], [28].

Fisher's method is effective when many p-values are small, as the logarithmic transform emphasizes lower values. However, it can be dominated by one or two extreme p-values, which makes it less robust in the presence of noise or partial signal corruption [27], [28].

2) HARMONIC MEAN P-VALUE (HMP)

The Harmonic Mean P-value provides a robust alternative that is less sensitive to small p-values than Fisher's method and allows for more balanced aggregation when the signal is weak. One of the key advantages of the HMP methods is its robustness to positive dependence among the combined tests [29], unlike Fisher's method which assumes independence and may inflate false positives when this assumption is violated. Given k p-values, the HMP is computed as:

$$HMP = (\frac{1}{k}\sum_{i=1}^{k}\frac{1}{p_i})^{-1} \tag{7}$$

This metric behaves similarly to the minimum p-value, but incorporates all available tests in a way that reduced the impact of outliers or violations of independence. The HMP is particularly useful when there is a mix of weak and strong signals across different tests [29].

When selecting a p-value fusion method, it is important to consider the assumptions made about the statistical relationship between the tests. Fisher's method performs optimally under the assumption of independence, making it a powerful choice when individual tests operate on unrelated or orthogonal features. However, in scenarios where tests may exhibit positive dependence, the HMP method provides a more robust alternative. In such cases, relying solely on Fisher's method may result in inflated significance levels, while HMP offers a more conservative and reliable aggregation. Including both methods in a detection framework can therefore offer a balance between sensitivity and robustness across a range of test correlation structures.

E. CONFUSION MATRIX AND EVALUATION METRICS

Evaluating the effectiveness of a nonstationarity detection system requires a rigorous and interpretable framework for assessing classification performance. In this work, the system's output for each signal is binary: the signal is either classified as stationary or nonstationary. To evaluate how these prediction align with known signals, we use the confusion matrix, a standard tool in binary classification tasks [30].

The confusion matrix for binary classification provides a summary of the prediction results and is defined by four components:

- True Positives (TP): The number of signals correctly identified as nonstationary. These are the cases where the detector successfully captures a transition event when one is actually present in the signal.
- True Negatives (TN): The number of signals correctly identified as stationary. These cases indicate correct acception of the null hypothesis when no transition or abnormality is present.
- False Positives (FP): The number of stationary signals incorrectly classified as nonstationary. This represents a type I error, where the algorithm falsely flags a nonstationarity in the signal when it is, in fact, stationary.
- False Negatives (FN): The number of nonstationary signals incorrectly classified as stationary. This corresponds to a type II error, where the detector fails to identify a real nonstationary event.

From these classifications, several metrics can be derived to provide insight into different aspects of the system performance such as:

1) ACCURACY

Accuracy measures the proportion of all correct predictions relative to the total number of trials. It gives an overall sense of how reliable the detection system is across all types of signals. It can be measured using:

$$Accuracy = \frac{TP + TN}{TP + TN + FP + FN} \tag{8}$$

Although high accuracy is desirable, it can be misleading in unbalanced datasets where one class dominates [30].

2) FALSE POSITIVE RATE (FPR)

The false positive rate quantifies how often the algorithm mistakenly labels a stationary signal as nonstationary. Calculated as:

$$FPR = \frac{FP}{FP + TN} \tag{9}$$

This metric is critical in industrial applications where false alarms can lead to unnecessary inspections, production delays, or loss of confidence in the monitoring system [30].

3) FALSE NEGATIVE RATE (FNR)

The false negative rate measures how often the algorithm misses an actual nonstationary event. Found using:

$$FNR = \frac{FN}{FN + TP} \tag{10}$$

This is perhaps the most crucial metric in predictive maintenance. A high FNR means that the system is failing to detect true anomalies, which can lead to unplanned failures or damage. Minimizing the FNR is essential for maintaining the safety and reliability of monitored equipment [30].

4) TRADE-OFFS AND PRACTICAL CONSIDERATIONS

The choice of decision threshold α directly affects the balance between FPR and FNR. A lower threshold results in more conservative decisions. reducing the chance of false positives at the cost of potentially missing weak nonstationary events. Conversely, a higher threshold increases sensitivity but may produce more false alarms [30].

III. PROPOSED DETECTION PIPELINE

This section provides an overview of the methodology developed to detect non-stationarities in motor current signals. The approach is based on statistical hypothesis testing applied to extract features from segments of signals. It covers the windowing steps, feature extraction, statistical testing, adaptive buffering, simulations setup, and validation on real motor datasets.

A. MOTOR CURRENT SIGNATURE ANALYSIS (MCSA) AND FAULT FREQUENCIES

Motor Signature Analysis (MCSA) is a non-invasive technique used to detect electrical and mechanical faults in motors by analysing the frequency spectrum of the stator current. When faults are present, they cause characteristic modulations in the current, producing frequency components - known as fault signatures - that deviate from the normal supply frequency.

Each type of fault introduces specific frequency patterns such as:

- Broken rotor bars generate sidebands around the supply frequency f_s at:

$$f_{bar} = (1 \pm 2ks)f_s \tag{11}$$

  where k is any positive integer [1], [31], [9], [32].

- Air gap eccentricity, caused by misalignment or rotor deformation, leads to components at:

$$f_{ecc} = ((kR \pm n_d)\frac{1-s}{p} \pm \nu)f_s \tag{12}$$

  where R is the number of rotor slots, s is the rotor slip, p is the number of pole pairs, k is any positive integer, n_d is the eccentricity order, and ν is the order of stator harmonics [1], [31] [9], [32].

- Bearing faults results in certain vibration which influences the eccentricity in air gap between the rotor and stator. Since the bearing vibration leads to ripple in output torque of the motor, it can be found in the current spectrum as:

$$f_{br} = |f_s \pm nf_c| \tag{13}$$

  where n is an integer and f_c is the characteristic vibration frequency of cage failure [1], [31], [9], [32].

- Stator winding faults create asymmetries in the magnetic field, typically leading to negative-sequence components and harmonics of f_s and f_r, computed as:

$$f_{st} = [k \pm \frac{n(1-s)}{p}]f_s \tag{14}$$

  where k is an odd integer, s is the rotor slip and p is the number of pole pairs [1], [31], [9], [32].

MCSA is widely used in industry due to its simplicity, low cost, and ability to monitor machines under load without physical intrusion. However, accurate interpretation of the spectral content is essential for reliable fault diagnosis.

B. SIGNAL WINDOWING AND FEATURE EXTRACTION

The input to the detection framework consists of time-domain current signals obtained either from Monte Carlo simulation or real-world acquisition. In both cases, the signals represent the stator phase current of an induction motor operating under potentially varying load conditions.

Each signal tested was sampled at 11.718 kHz, and consists of 262144 samples, corresponding to approximately 22 seconds of data.

To allow for localized statistical analysis and to avoid assumptions of stationarity over long periods, each signal is partitioned into 512 non-overlapping windows of equal length, resulting 512 consecutive samples per window. This segmentation ensures sufficient temporal resolution to detect brief nonstationary events, while maintaining a manageable number of samples per window to compute stable statistics. The window length was selected empirically based on exploratory testing: larger windows yielded more stable feature estimates but reduced temporal resolution, which in turn made short-duration nonstationary events harder to detect, lowering detection accuracy. In contrast, smaller windows improved temporal granularity but led to worse statistical descriptors due to fewer samples per window, and also increased computational cost by requiring more frequent hypothesis testing. The chosen window size therefore reflects a practical trade-off between sensitivity to local changes, statistical reliability of the features, and overall computational efficiency.

Additionally, non-overlapping windows were chosen to preserve approximate statistical independence between consecutive data segments. Although the statistical tests used in this work are applied to features extracted from each window rather than to raw samples, overlapping windows could still introduce correlation between adjacent feature vectors due to shared samples. This feature-level dependence may compromise the validity of the independence assumption

underlying these tests, potentially biasing their outcomes or inflating false positive rates. By avoiding overlap, we reduce the likelihood of such artifacts and ensure that each window's feature vector reflects an independent observation of the signal's local statistical behaviour.

For each window, four statistical descriptor are calculated:

- Mean: Estimates the average amplitude level of the window.
- Variance: Captures the energy or dispersion of the signal.
- Skewness: Measures the asymmetry of the distribution, useful for identifying shifts or lopsided behaviour.
- Kurtosis: Quantifies the ''taildness'' of the distribution, capturing spiky or flat-top behaviour.

The choice of these metrics was driven by their simplicity, low computational cost, and ability to succinctly describe the probability distribution of the signal within each window, making them well-suited for nonparametric hypothesis testing. While more complex descriptors such as entropy or fractal dimension may offer higher sensitivity in some contexts, they are also significantly more sensitive to small variations or noise that can lead to false positives when used with robust nonparametric tests.

These features are concatenated to form a feature vector per window. The result is a feature matrix of shape (512, 4) representing the entire signal in feature space. These descriptors are chosen for their computational simplicity and their capacity to represent dynamic changes in signal behaviour without reliance on time-frequency transforms.

C. ADAPTIVE BUFFERING BASED ON WASSERSTEIN DISTANCE

To evaluate whether a window deviates from normal signal behaviour, it is compared against a reference buffer containing feature vectors from earlier windows. Rather than using a fixed-size buffer, the method employs an adaptive buffer strategy to tailor the comparison scope to each signal's internal variability.

The first-order Wasserstein distance is used to quantify variability between adjacent windows and the average distance between all consecutive windows is normalized by 95th percentile distance and scaled between a maximum and minimum buffer sizes. This allows the buffer to expand for more variable signals, to better capture its dynamics, and shrink to more stable signals to reduce the computational cost. Unlike the statistical tests applied later in the pipeline, which operate on the feature vector of the windows, the Wasserstein Distance is computed directly on the raw samples distributions of each window. This provides a sensitive measure of local distributional variation in the signal itself.

D. STATISTICAL HYPOTHESIS TESTING OF WINDOW FEATURES

Once the reference buffer is established, the current window's feature vector is tested for statistical deviation from the buffer using three nonparametric hypothesis tests - Anderson-Darling, Kolmogorov-Smirnov and Cramér-von Mises.

Each test compares the current feature vector with those in the buffer, returning a p-value representing the probability that the current window probability distribution function has a considerable deviation from the previously observed.

To enhance reliability, the Fisher's method and Harmonic Mean P-value fusion methods are performed on the p-values of the three tests, generating two more. Each p-value is compared against a threshold α and, if it is lower, the window is flagged as nonstationary.

A final majority decision is also deployed that gives the classification of the majority of the tests. Hence, if at least three out of five p-values of one window falls below α the majority test will flag it as nonstationary, and stationary otherwise.

While a weighted decision based on sensitivity could provide a more nuanced decision, it would require prior knowledge of each test's relative performance under the imposed signal conditions to establish static weights, which may lead to suboptimal or biased decisions, or estimation of each test relevance dynamically at the cost of computational complexity. In contrast, the binary majority voting provides a transparent and assumption-free way to integrate test outcomes, favouring robustness and interpretability.

E. SIMULATIONS SETUP

To rigorously evaluate the proposed nonstationarity detection framework, a series of Monte Carlo simulations was conducted using both $\alpha = 0.01$ and 0.05 as the standard threshold values for hypothesis testing. These simulations were designed to replicate realistic electrical and mechanical behaviours commonly observed in induction motors, capturing both operational variability and fault-like disturbances. The experiments focused on two distinct types of nonstationary - global and local - allowing the system to be tested under both persistent and transient dynamic changes.

For each type of nonstationarity, 1000 trials were simulated and, for each simulation trial, a generated synthetic motor current signal of approximately 22 seconds sampled at 11.718 kHz using randomized parameters, with a 50% chance of being either stationary or nonstationary. This ensures a balanced dataset for evaluating the system's statistical power and robustness without introducing a performance bias.

The signals were constructed by independent sampling a set of parameters from uniform distributions over realistic physical ranges:

- Fundamental frequency (f_0): Simulates power supply fundamental frequency. Drawn uniformly from 58 Hz to 62 Hz;
- Rotational slip (s): Models rotor speed deviation. Sampled uniformly from 0.35 to 0.95;
- Amplitude of the Fundamental Component (A_0): Represents signal strength. Ranges from 1.0 to 5.0;

- Harmonic Amplitude (A_{har}): Adds harmonic waveform distortion. Ranges from 0.5 to 2.5;
- Fault-related Sideband Amplitudes (A_{pp}, A_{bars}): Simulates mechanical faults such as broken bars or eccentricities. Drawn from 0.2 to 0.8;
- Additive Gaussian Noise (σ_{noise}): Reflects measurement noise or environmental interference. Standard deviation sampled from 0.01 to 0.1;
- Phase Angles: Randomly selects one of the current phase of the motor;
- Number of Poles: Chosen from the set 2. 4. 6;
- Number of Rotor Bars: Drawn from the even integers between 4 and 40, simulating rotor geometry diversity.

In the case of stationary signals, all parameters remained constant throughout the entire duration. For nonstationary trials, a second set of parameter values was samples, except the Gaussian noise, phase angles, number of poles and rotor bars. These values were linearly interpolated from the initial to the final value over the relevant time interval, enabling controlled signal evolution. The choice of using uniform probability distributions and a 50% chance of a nonstationarity occurring is made such that all possible parameter combinations have equal chance of being tested, creating a balanced dataset. An unbalanced dataset would induce a simulation bias, skewing the results.

The resulting signals were analysed using the statistical detection procedure described in previous sections. Simulations were conducted under two distinct nonstationarity regimes, detailed below.

1) GLOBAL NONSTATIONARY SIMULATIONS

In this configuration, the nonstationary behaviour spans the full length of the signal. The regime simulates slow but consistent changes in the motor's operating state - such as long-term variations in load, rotor speed, or voltage supply - which may manifest as gradual drifts in the statistical structure of the current signal.

The objective of this regime was to assess the system's sensitivity to broad, sustained deviations in signal dynamics. Since the data was fully synthetic, ground truth labels were known, enabling precise computation of the classification metrics discussed previously.

2) LOCAL NONSTATIONARY SIMULATIONS

In this regime, the nonstationarity is confined to a limited time window within the signal - emulating sudden, short-lived events such as transient faults or step changes in mechanical load. This is a more difficult detection task because the nonstationary behaviour is surrounded by statistically stationary intervals. For nonstationary cases, the transient interval was defined by sampling two time points:

- Start time (t_{start}): Chosen uniformly between 5 and 7 seconds;
- End time (t_{end}): Chosen uniformly between 13 and 17 seconds.

Within this interval, the parameters evolved linearly from their initial to final values, while remaining stationary outside it. Stationary signals again held all parameters constant for the entire duration.

This simulation setup tested not only the system's ability to identify the presence of nonstationary dynamics, but also its robustness in avoiding false alarms during unaffected regions.

F. REAL MOTOR SIGNAL VALIDATION

To assess the performance of the proposed nonstationarity detection framework in real-world conditions, it was applied to a dataset of 529 motor current signals collected from a submerged BCS water transfer pump model SCH_750HP with 2 poles, rotation speed of 3570 RPM, power of 750 HP, input tension of 2278C and current of 200 A, operating under industrial conditions. The dataset spans a period of roughly three months, with one signal acquire every six hours. This long-term monitoring campaign enabled the observation of both gradual system drifts and occasional transient disturbances. All signals measured passed through a decision algorithm that checked if variations in the instant frequency were greater than a specified threshold, if so the signal was discarded and didn't become part of the dataset.

Each acquisition contained all three phase currents (I_a, I_b and I_c), each sampled 11.718 kHz and lasting approximately 22 seconds - matching the configuration used in the synthetic simulations. All phases were initially analysed using the full detection procedure described previously.

Nonstationary behaviour, when present, tends to manifest simultaneously across all three phases due to inherent symmetry of induction motors and the shared influence of rotor dynamics on each phase current. In particular, rotoric-related phenomena such as slip variation and fault-induced frequencies appear coherently across all phases. This redundancy provided confidence in the detection results and enabled phase selection for simplified reporting. Consequently, the analysis of this work focuses on phase A (I_a), both for clarity and because its behaviour was representative of the general system dynamics observed across the other two phases during exploratory evaluation. While a formal cross-phase analysis was not conducted, no significant divergence in nonstationarity patterns was observed, supporting the decision to focus on a single phase.

Since the real signals lacked ground-truth labels indicating the presence or absence of nonstationary events, the validation of the detection algorithm relied on indirect and domain-informed metrics. The core of the evaluation was based on the behaviour of the static eccentricity spectral band, which is known to be sensitive to underlying nonstationarities.

The real-world signals were evaluated using the same α as the simulations and in the range from 0.06 to 0.2 to demonstrate the proposed method performance and how this free parameter affects its sensitivity, tolerance and results.

TABLE 1. Anderson-darling results for global nonstationarities simulations.

α:	0.01
TP: 471	FN: 0
FP: 110	TN: 419
Accuracy:	89%
FPR:	20.8%
FNR:	0%

α:	0.05
TP: 501	FN: 0
FP: 146	TN: 353
Accuracy:	85.4%
FPR:	29.3%
FNR:	0%

IV. PROCESS EVALUATION

This section presents and interprets the results obtained from the proposed nonstationarity detection framework applied to both synthetic and real-world motor current signals. The method's applicability to real-world signals were assessed by analysing the spectral spread of fault-sensitive frequency band of the static eccentricity as well as its trend along the time.

A. GLOBAL NONSTATIONARY

Tables 1-6 summarize the performance of all tested statistical approaches under globally nonstationary signal conditions with both $\alpha = 0.01$ and 0.05. Across all 1000 Monte Carlo trials, all tests correctly identified nonstationary signals (true positives) with perfect recall, evidenced by a 0% false negative rate in every case.

The Cramér-von Mises Test exhibited the highest accuracy at 94.1% for $\alpha = 0.01$, as shown in Table 3. This test also maintained the lowest false positive rate at 11.2% indicating its strong discriminative ability for stationary versus globally nonstationary signals.

Similarly, the Harmonic Mean P-value fusion method achieved an accuracy of 93.3% under the same threshold with comparable false positive rate of 12.7%, as shown in Table 5. The majority vote classifier yielded a consistent performance of 93.1%, as in Table 6, suggesting the ensemble benefits from combining different test sensitivities.

The Kolmogorov-Smirnov test also showed strong performance, reaching 92.6% accuracy with a 13.9% false positive rate at $\alpha = 0.01$, as demonstrated in Table 2. When the threshold increased to $\alpha = 0.05$, the accuracy dropped to 86.3%, and the false positive rate rose to 27.5%, reflecting the expected trade-off introduced by a more permissive significance level.

On contrary, Fisher's method and Anderson-Darling test showed significantly higher false positive rates, at 30.1% and 20.8%, respectively, leading to overall accuracies of 84.1% 89%. This trend was exacerbated under $\alpha = 0.05$, with Fisher's method degrading to 80.5%, as in Table 4 and Table 1 respectively.

B. LOCAL NONSTATIONARY

Detection performance under localized nonstationarity conditions is summarized in Tables 7-12. This scenario introduced a more subtle classification challenge.

Despite this, the CvM test again led in accuracy, achieving 95.8% at $\alpha = 0.01$ with remarkably low 7.7% false positive rate, as in Table 9. The HMP method also excelled in this context with 95.9% accuracy and a false positive rate of 8.3%, shown in Table 11. These figures represent the best results across the entire study and highlight the robustness of these methods in detecting localized time-varying behaviour.

TABLE 2. Kolmogorov-Smirnov results for global nonstationarities simulations.

α:	0.01
TP: 471	FN: 0
FP: 74	TN: 455
Accuracy:	92.6%
FPR:	13.9%
FNR:	0%

α:	0.05
TP: 501	FN: 0
FP: 137	TN: 362
Accuracy:	86.3%
FPR:	27.5%
FNR:	0%

TABLE 3. Cramér-von Mises results for global nonstationarities simulations.

α:	0.01
TP: 471	FN: 0
FP: 59	TN: 470
Accuracy:	94.1%
FPR:	11.2%
FNR:	0%

α:	0.05
TP: 501	FN: 0
FP: 106	TN: 393
Accuracy:	89.4%
FPR:	21.2%
FNR:	0%

TABLE 4. Fisher's method results for global nonstationarities simulations.

α:	0.01
TP: 471	FN: 0
FP: 159	TN: 370
Accuracy:	84.1%
FPR:	30.1%
FNR:	0%

α:	0.05
TP: 501	FN: 0
FP: 195	TN: 304
Accuracy:	80.5%
FPR:	39.1%
FNR:	0%

TABLE 5. Harmonic mean p-value results for global nonstationarities simulations.

α:	0.01
TP: 471	FN: 0
FP: 67	TN: 462
Accuracy:	93.3%
FPR:	12.7%
FNR:	0%

α:	0.05
TP: 501	FN: 0
FP: 119	TN: 380
Accuracy:	88.1%
FPR:	23.8%
FNR:	0%

TABLE 6. Majority decision results for global nonstationarities simulations.

α:	0.01
TP: 471	FN: 0
FP: 69	TN: 460
Accuracy:	93.1%
FPR:	13%
FNR:	0%

α:	0.05
TP: 501	FN: 0
FP: 124	TN: 375
Accuracy:	87.6%
FPR:	24.9%
FNR:	0%

TABLE 7. Anderson-darling results for local nonstationarities simulations.

α:	0.01
TP: 521	FN: 0
FP: 70	TN: 409
Accuracy:	93%
FPR:	14.6%
FNR:	0%

α:	0.05
TP: 496	FN: 0
FP: 170	TN: 334
Accuracy:	83%
FPR:	33.7%
FNR:	0%

TABLE 8. Kolmogorov-Smirnov results for local nonstationarities simulations.

α:	0.01
TP: 521	FN: 0
FP: 51	TN: 428
Accuracy:	94.9%
FPR:	10.6%
FNR:	0%

α:	0.05
TP: 496	FN: 0
FP: 154	TN: 350
Accuracy:	84.6%
FPR:	30.6%
FNR:	0%

TABLE 9. Cramér-von mises results for local nonstationarities simulations.

α:	0.01
TP: 516	FN: 5
FP: 37	TN: 442
Accuracy:	95.8%
FPR:	7.7%
FNR:	0.9%

α:	0.05
TP: 496	FN: 0
FP: 112	TN: 392
Accuracy:	88.8%
FPR:	22.2%
FNR:	0%

TABLE 10. Fisher's method results for local nonstationarities simulations.

α:	0.01
TP: 521	FN: 0
FP: 116	TN: 363
Accuracy:	88.4%
FPR:	24.2%
FNR:	0%

α:	0.05
TP: 496	FN: 0
FP: 218	TN: 286
Accuracy:	78.2%
FPR:	43.3%
FNR:	0%

TABLE 11. Harmonic mean p-value results for local nonstationarities simulations.

α:	0.01
TP: 520	FN: 1
FP: 40	TN: 439
Accuracy:	95.9%
FPR:	8.3%
FNR:	0.2%

α:	0.05
TP: 496	FN: 0
FP: 144	TN: 360
Accuracy:	85.6%
FPR:	28.6%
FNR:	0%

TABLE 12. Majority decision results for local nonstationarities simulations.

α:	0.01
TP: 520	FN: 1
FP: 43	TN: 436
Accuracy:	95.6%
FPR:	8.9%
FNR:	0.2%

α:	0.05
TP: 496	FN: 0
FP: 146	TN: 358
Accuracy:	85.4%
FPR:	28.9%
FNR:	0%

The majority vote classifier once more performed competitively, recording 95.6% accuracy at $\alpha = 0.01$ only marginally trailing the best individual methods, as in Table 12.

In contrast, Fisher's method again underperformed, with a high 24.2% false positive rate at $\alpha = 0.01$ and a steep decline in accuracy to 78.2% as well as the increase in the false positive rate to 43.3% when the threshold was increased to $\alpha = 0.05$, as in Table 10. The AD and KS tests improved over the global case, accuracy of 93% and 94.9% as demonstrated in Table 7 and Table 8, respectively, but still lagged behind the top performers.

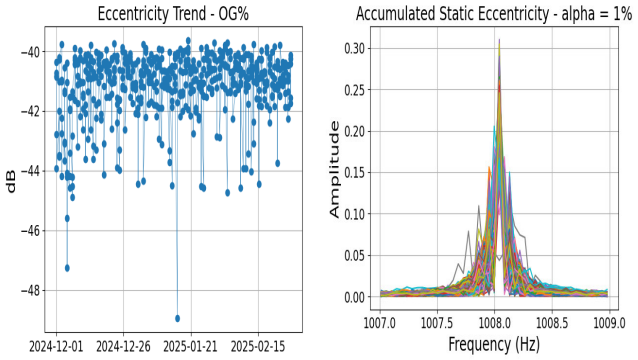

Mean: -41.159 dB Std: 1.151 dB

FIGURE 1. Original dataset static eccentricity trend and accumulated spectra.

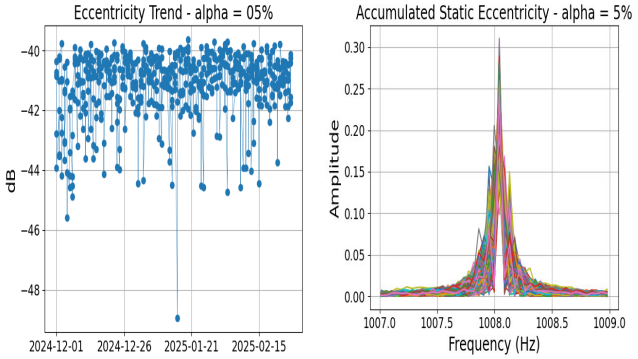

Mean: -41.142 dB Std: 1.114 dB

FIGURE 2. Dataset static eccentricity trend and accumulated spectra for $\alpha = 0.05$.

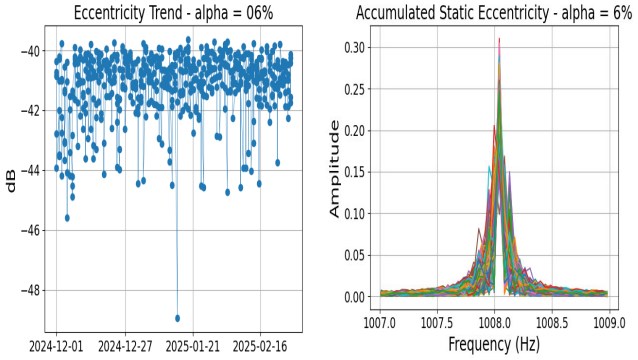

Mean: -41.135 dB Std: 1.106 dB

FIGURE 3. Dataset static eccentricity trend and accumulated spectra for $\alpha = 0.06$.

C. REAL MOTOR SIGNALS

To assess its practical effectiveness, the method was applied with varying significance threshold, and its impact on the spectral spread of the static eccentricity band was analysed. This band is particularly sensitive to rotor speed variations,

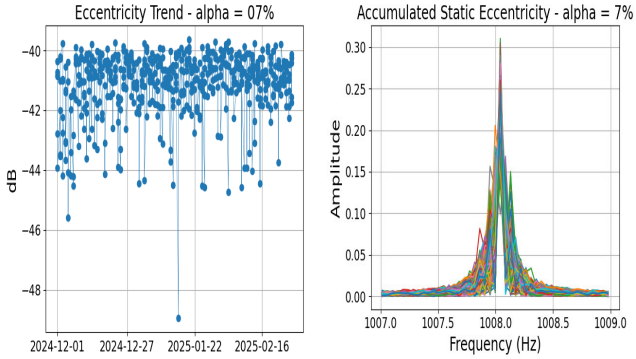

Mean: -41.123 dB Std: 1.090 dB

FIGURE 4. Dataset static eccentricity trend and accumulated spectra for $\alpha = 0.07$.

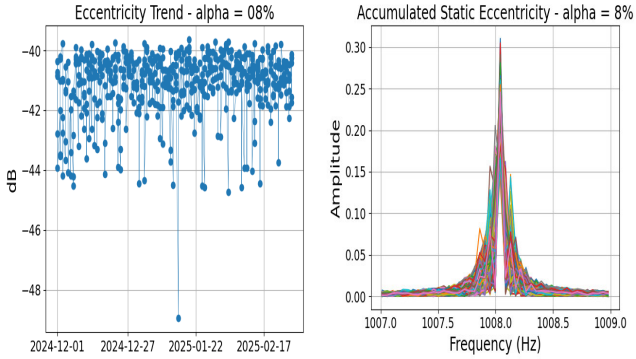

Mean: -41.108 dB Std: 1.068 dB

FIGURE 5. Dataset static eccentricity trend and accumulated spectra for $\alpha = 0.08$.

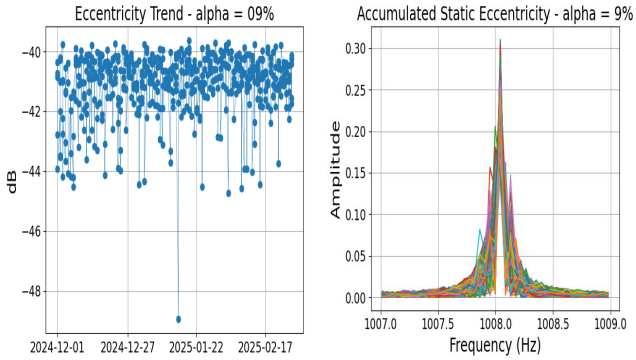

Mean: -41.095 dB Std: 1.051 dB

FIGURE 6. Dataset static eccentricity trend and accumulated spectra for $\alpha = 0.09$.

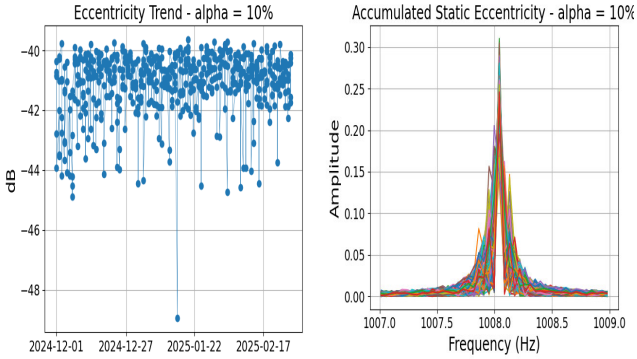

Mean: -41.106 dB Std: 1.066 dB

FIGURE 7. Dataset static eccentricity trend and accumulated spectra for $\alpha = 0.10$.

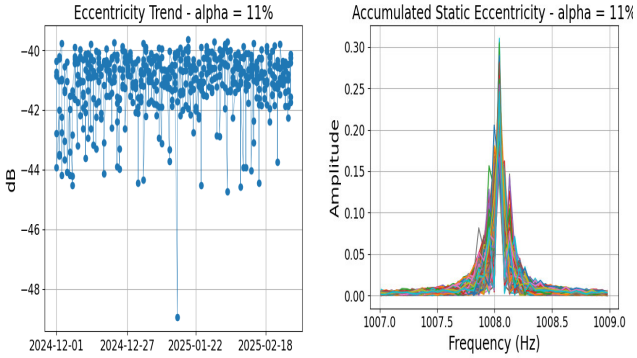

Mean: -41.099 dB Std: 1.052 dB

FIGURE 8. Dataset static eccentricity trend and accumulated spectra for $\alpha = 0.11$.

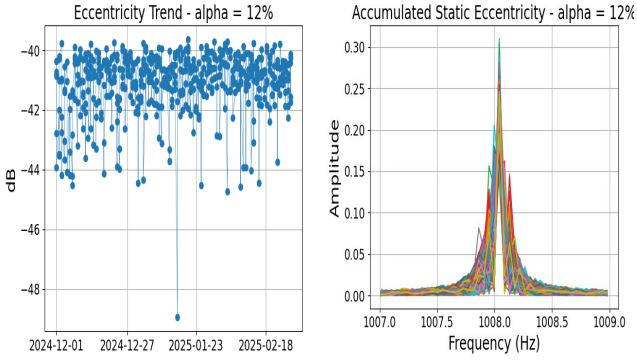

Mean: -41.099 dB Std: 1.052 dB

FIGURE 9. Dataset static eccentricity trend and accumulated spectra for $\alpha = 0.12$.

making it a reliable indirect indicator of nonstationary behaviour.

To quantify the method's influence on signal quality, the mean and standard deviation of the static eccentricity trend (in dB) and the accumulated spectra of the static eccentricity band of all signals were computed for the remaining signals after filtering the signals classified has nonstationary out, using different values of the significance threshold α. Specifically, tests were performed for $\alpha = 0.01$ and values ranging from 0.05 to 0.2 in 0.01 increments as shown in Figures 1-17.

At $\alpha = 0.01$, the method was extremely conservative, classifying all signals as stationary, making it identical to

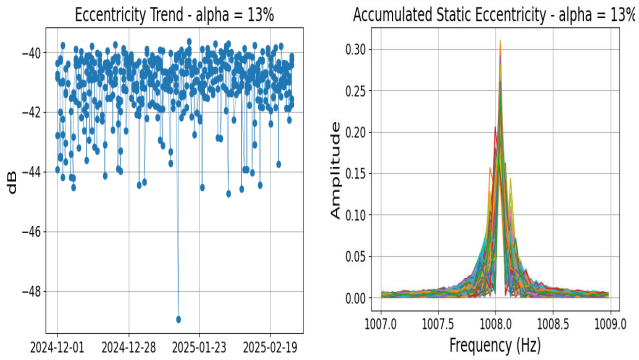

Mean: -41.094 dB Std: 1.046 dB

FIGURE 10. Dataset static eccentricity trend and accumulated spectra for $\alpha = 0.13$.

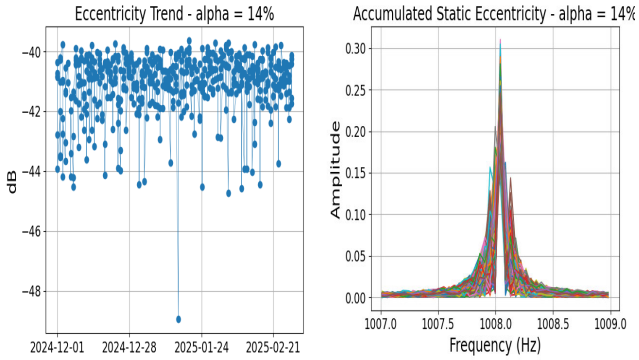

Mean: -41.081 dB Std: 1.037 dB

FIGURE 11. Dataset static eccentricity trend and accumulated spectra for $\alpha = 0.14$.

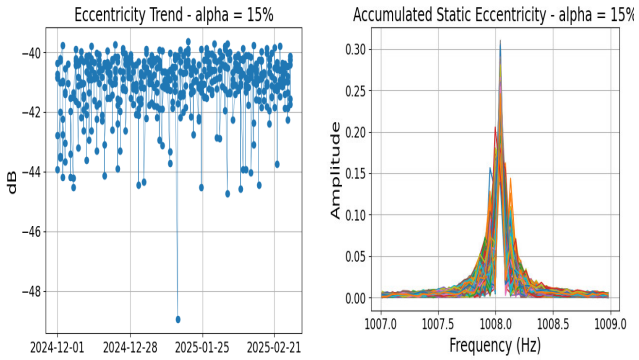

Mean: -41.083 dB Std: 1.039 dB

FIGURE 12. Dataset static eccentricity trend and accumulated spectra for $\alpha = 0.15$.

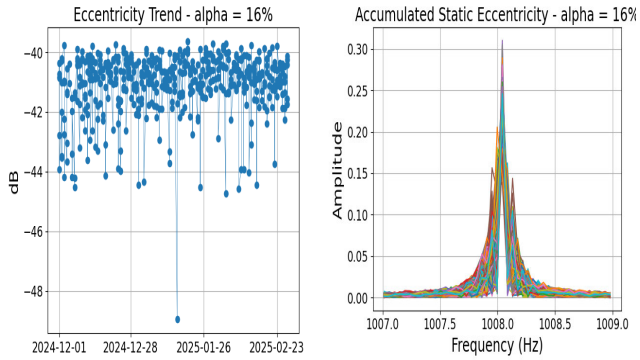

Mean: -41.088 dB Std: 1.053 dB

FIGURE 13. Dataset static eccentricity trend and accumulated spectra for $\alpha = 0.16$.

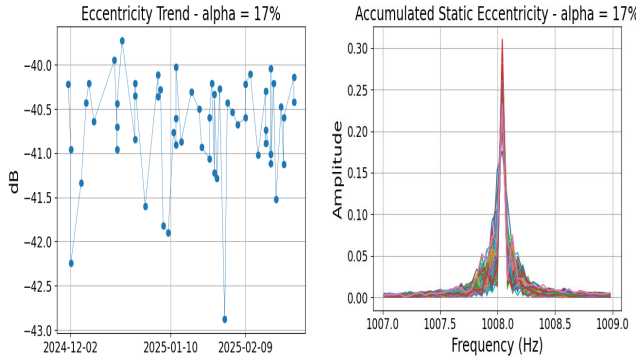

Mean: -40.705 dB Std: 0.587 dB

FIGURE 14. Dataset static eccentricity trend and accumulated spectra for $\alpha = 0.17$.

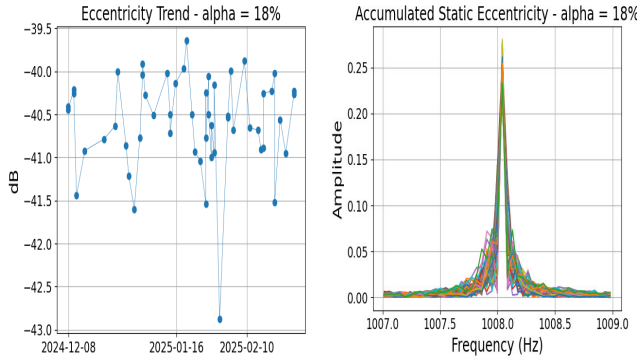

Mean: -40.588 dB Std: 0.549 dB

FIGURE 15. Dataset static eccentricity trend and accumulated spectra for $\alpha = 0.18$.

the unfiltered dataset, which has mean of -41.159 dB with standard deviation of 1.151 dB as in Figure 1.

As α increased from 0.05 to 0.16, the standard deviation of the static eccentricity trend gradually decreased, reaching a minimum of approximately 1.037 dB at $\alpha = 0.14$ as in Figure 11. This behaviour suggests that the method was increasingly effective at identifying and discarding signals exhibiting nonstationary traits, thus improving the concentration of energy in the expected frequency band, which can be observed in the accumulated spectra, where they appear more homogeneous.

Beyond $\alpha = 0.16$, the results began to show diminishing returns. Although the standard deviation of the static eccentricity trend continued to decline - reaching 0.521 at

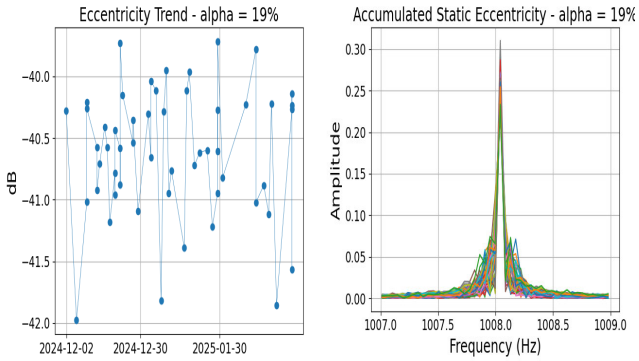

FIGURE 16. Dataset static eccentricity trend and accumulated spectra for $\alpha = 0.19$.

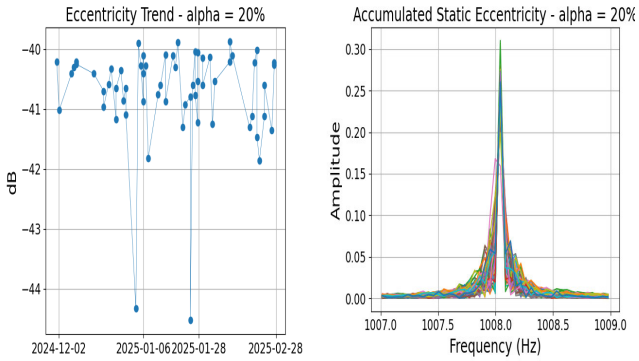

FIGURE 17. Dataset static eccentricity trend and accumulated spectra for $\alpha = 0.20$.

$\alpha = 0.19$ as shown in Figure 16 - this was accompanied by a noticeable drop in the number of signals remaining in the dataset. This behaviour indicates that the method became overly sensitive, classifying a growing number of stationary signals as nonstationary, inflating its false positive rate. This excessive filtering not only reduced the sample size available for downstream analysis but also introduces the risk of misrepresenting the motor's actual condition, potentially leading to an overly pessimistic assessment of the system health. Such behaviour underscores the importance of carefully selecting α to avoid compromising the dataset's representativeness.

V. CONCLUSION

This study presented a statistically grounded framework for detecting nonstationarities in motor current signals, avoiding reliance on complex signal decomposition or deep learning. Instead the method leverages statistical hypothesis testing on global statistical features computed across non-overlapping windows of the signal. Tests such as the 2-sample Anderson-Darling, Kolmogorov-Smirnov, and Cramér-von Mises were used individually and in combination through p-value fusion strategies, particularly Fisher's method and the Harmonic Mean P-value, were applied to make the classification decision.

Extensive Monte Carlo simulations demonstrated the method's accuracy reaches high values like 95.9% and its false negative rate is kept low never going above 0.5% across both global and local nonstationarity scenarios. Among all techniques, the HMP method and Cramér-von Mises test yielded the best overall performances.

Real-world validation on a dataset of 529 current signals of a BCS water pump confirmed the method's generalization capability to be used in different types of motors. By analysing the spread of the static eccentricity band, the method was able to identify unstable signals. An optimal significance level α was found around 14%, balancing sensitivity and false positive rates. Lower thresholds like $\alpha = 0.01$, although effective in simulations, proved too conservative for real signals, while values higher than $\alpha = 0.16$ led to excessive data rejection.

Its computational complexity is approximately O(n * m * log m), where n is the number of analysis windows and m is the number of samples per window, reflecting the cost of the repeated statistical testing and distribution comparisons, and a total memory usage of 1.32 MB. These results indicate that the memory maintains a low memory footprint and moderate computational cost, making it feasible for near real-time monitoring scenarios or deployment on resource-constrained platforms.

In summary, this work delivers an interpretable, low-cost, and statistically principled approach for real-time nonstationarity detection, offering a valuable tool for predictive maintenance and industrial condition monitoring. Future work could explore a nonstationary interval estimation using the p-values of each window and a Bayesian or Bootstrap window re-estimation to better approximate the exact time that the transient event started and ended.

ACKNOWLEDGMENT

Eduardo Vaz Fagundes Rech would like to thank the Federal University of Itajubá for the research scholarship.

REFERENCES

[1] G. Niu, X. Dong, and Y. Chen, "Motor fault diagnostics (Don't short) based on current signatures: A review," *IEEE Trans. Instrum. Meas.*, vol. 72, pp. 1–19, 2023.

[2] Z. Y. M. Hurtado, C. P. Tello, and J. G. Sarduy, "A review on detection and fault diagnosis in induction machines," *Publicaciones en Ciencias y Tecnologia*, vol. 8, pp. 11–30, Apr. 2014.

[3] D. Morinigo-Sotelo, R. De J. Romero-Troncoso, P. A. Panagiotou, J. A. Antonino-Daviu, and K. N. Gyftakis, "Reliable detection of rotor bars breakage in induction motors via MUSIC and ZSC," *IEEE Trans. Ind. Appl.*, vol. 54, no. 2, pp. 1224–1234, Mar. 2018.

[4] O. Ryan, J. M. B. Haslbeck, and L. J. Waldorp, "Non-stationarity in time-series analysis: Modeling stochastic and deterministic trends," *Multivariate Behav. Res.*, vol. 60, no. 3, pp. 556–588, May 2025.

[5] J. E. Garcia-Bracamonte, J. M. Ramirez-Cortes, J. de Jesus Rangel-Magdaleno, P. Gomez-Gil, H. Peregrina-Barreto, and V. Alarcon-Aquino, "An approach on MCSA-based fault detection using independent component analysis and neural networks," *IEEE Trans. Instrum. Meas.*, vol. 68, no. 5, pp. 1353–1361, May 2019.

[6] X. Song, Z. Wang, and J. Hu, "Detection of bearing outer race fault in induction motors using motor current signature analysis," in *Proc. Int. Conf. Electr. Mach. Syst.*, 2019, pp. 1–5.
[7] I. Zamudio-Ramirez, J. J. Saucedo-Dorantes, J. Antonino-Daviu, R. A. Osornio-Rios, and L. Dunai, "Detection of uniform gearbox wear in induction motors based on the analysis of stray flux signals through statistical time-domain features and dimensionality reduction techniques," *IEEE Trans. Ind. Appl.*, vol. 58, no. 4, pp. 4648–4656, Jul. 2022.
[8] P. Yelpale, R. K. Jarial, and A. J. Patil, "Fuzzy-based induction motor fault diagnosis decision-making system for motor current signature analysis," in *Proc. Int. Conf. Innov. Technol.*, Mar. 2024, pp. 1–6.
[9] D. Liu, H. Inoue, and M. Kanemaru, "Robust motor current signature analysis (MCSA)-based fault detection under varying operating conditions," in *Proc. 25th Int. Conf. Electr. Mach. Syst. (ICEMS)*, Nov. 2022, pp. 1–5.
[10] Y. Li, H. Zhao, W. Fan, and C. Shen, "Generalized autocorrelation method for fault detection under varying-speed working conditions," *IEEE Trans. Instrum. Meas.*, vol. 70, pp. 1–11, 2021.
[11] D. B. de Souza, J. Chanussot, A.-C. Favre, and P. Borgnat, "A new nonparametric method for testing stationarity based on trend analysis in the time marginal distribution," in *Proc. IEEE Int. Conf. Acoust., Speech Signal Process. (ICASSP)*, May 2014, pp. 320–324.
[12] Y. Chu and C. M. Mak, "A new parametric adaptive nonstationarity detector and application," *IEEE Trans. Signal Process.*, vol. 65, no. 19, pp. 5203–5214, Oct. 2017.
[13] H. Amoud, P. Honeine, C. Richard, P. Borgnat, and P. Flandrin, "Time-frequency learning machines for nonstationarity detection using surrogates," in *Proc. IEEE/SP 15th Workshop Stat. Signal Process.*, Aug. 2009, pp. 565–568.
[14] Z. Zhu, S. Kay, F. Cogun, and R. S. Raghavan, "On detection of nonstationarity in radar signal processing," in *Proc. IEEE Radar Conf. (RadarConf)*, May 2016, pp. 1–4.
[15] E. M. Khadidja, B. Hadjira, and M. Abdelkrim, "The effect of the width of nonstationary spikes on their detection using Kalman filter," in *Proc. 7th Int. Conf. Image Signal Process. Appl. (ISPA)*, Mostaganem, Algeria, May 2022, doi: 10.1109/ISPA54004.2022.9786329.
[16] H. Sun, S. Zhang, C. Zhao, and Y. Sun, "Fault isolation method for nonstationary industrial processes," in *Proc. 29th Chin. Control Decision Conf.*, May 2017, pp. 6637–6642.
[17] F. Tian, C. Zhao, H. Fan, W. Zheng, and Y. Sun, "Fault diagnosis based on EEMD and key feature representation with separation of stationary and nonstationary signals," in *Proc. CAA Symp. Fault Detection, Supervision Saf. Tech. Processes*, Jul. 2019, pp. 29–34.
[18] H. Ozkan, F. Ozkan, and S. S. Kozat, "Online anomaly detection under Markov statistics with controllable type-I error," *IEEE Trans. Signal Process.*, vol. 64, no. 6, pp. 1435–1445, Mar. 2016.
[19] S. Kolouri, S. R. Park, M. Thorpe, D. Slepcev, and G. K. Rohde, "Optimal mass transport: Signal processing and machine-learning applications," *IEEE Signal Process. Mag.*, vol. 34, no. 4, pp. 43–59, Jul. 2017.
[20] A. Ramdas, N. Trillos, and M. Cuturi, "On Wasserstein two-sample testing and related families of nonparametric tests," *Entropy*, vol. 19, no. 2, p. 47, Jan. 2017.
[21] A. N. Pettitt, "A two-sample anderson-darling rank statistic," *Biometrika*, vol. 63, no. 1, pp. 161–168, Apr. 1976.
[22] F. W. Scholz and M. A. Stephens, "K-sample anderson-darling tests," *J. Amer. Stat. Assoc.*, vol. 82, no. 399, pp. 918–924, Sep. 1987.
[23] M. Golz, V. Koivunen, and A. Zoubit, "Nonparameric etection using empirical distribution and bootstrapping," in *Proc. 25th Eur. Signal Process. Conf.*, 2017, doi: 10.23919/EUSIPCO.2017.8081449.
[24] C. Wang, B. Zeng, and J. Shao, "Application of bootstrap method in Kolmogorov–Smirnov test," in *Proc. Int. Conf. Qual., Rel., Risk, Maintenance, Saf. Eng.*, Jun. 2011, pp. 287–291.
[25] J. Kiefer, "K-Sample analogues of the Kolmogorov–Smirnov and Cramérvon Mises tests," *Ann. Math. Statist.*, vol. 30, no. 2, pp. 420–447, Jun. 1958.
[26] T. W. Anderson, "On the distribution of the two-sample Cramer-von Mises criterion," *Ann. Math. Statist.*, vol. 33, no. 3, pp. 1148–1159, Sep. 1962.
[27] J. T. Kost and M. P. McDermott, "Combining dependent P-values," *Statist. Probab. Lett.*, vol. 60, no. 2, pp. 183–190, Nov. 2002.
[28] T. Halme, V. Koivunen, and H. V. Poor, "Nonparametric distributed detection using bootstrapping and Fisher's method," in *Proc. 52nd Annu. Conf. Inf. Sci. Syst. (CISS)*, Mar. 2018, pp. 1–6.
[29] D. J. Wilson, "The harmonic mean P-value for combining dependent tests," *Proc. Nat. Acad. Sci. USA*, vol. 116, no. 4, pp. 1195–1200, Jan. 2019.
[30] D. M. W. Powers, "Evaluation: From precision, recall and F-factor to ROC, informedness, markedness & correlation," School Inform. Eng., Flinders Univ., Adelaide, Australia, Tech. Rep. SIE-07-001, Dec. 2007.
[31] S. Kumar, D. Mukherjee, P. K. Guchhait, R. Banerjee, A. K. Srivastava, D. N. Vishwakarma, and R. K. Saket, "A comprehensive review of condition based prognostic maintenance (CBPM) for induction motor," *IEEE Access*, vol. 7, pp. 90690–90704, 2019.
[32] C. P. Salomon, C. Ferreira, G. Lambert-Torres, C. E. Teixeira, L. E. B. da Silva, W. C. Santana, E. L. Bonaldi, and L. E. L. de Oliveira, "Electrical signature analysis for condition monitoring of permanent magnet synchronous machine," *Adv. Electr. Comput. Eng.*, vol. 18, no. 4, pp. 91–98, Nov. 2018.

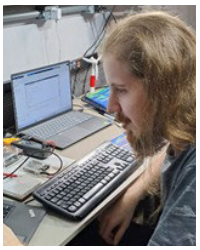

EDUARDO VAZ FAGUNDES RECH received the degree in computer engineering from the University of Brasilia (UNB), Brasília, Brazil, in 2023. He is currently pursuing the master's degree in electrical engineering with the Federal University of Itajubá (UNIFEI), Brazil.

He has been with CGRECH Informatica, Brasilia. He is also a Researcher with the Gnarus Institute, Itajubá, Brazil. His professional interests include development of hardware, firmware, software and operational systems for automation, robotics, and embedded systems, focusing on biomedicine, energy, aerospace, and industrial systems.

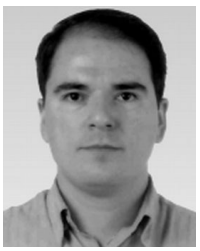

LEVY ELY DE LACERDA DE OLIVEIRA received the B.S., M.Sc., and D.Sc. degrees in electrical engineering from the Federal University of Itajubá, Itajubá, Brazil, in 1999, 2002, and 2006, respectively.

He is currently the CTO of PS Solutions and a Research Associate with the Gnarus Institute. He has experience with development of electronic systems (hardware, firmware, and software) for monitoring of electric machinery. His research interests include data acquisition systems, digital signal processing, and microcontrollers.

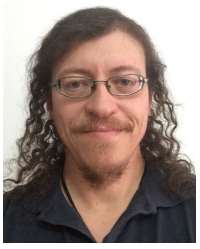

WILSON CESAR SANT'ANA (Senior Member, IEEE) received the B.S., M.Sc., and D.Sc. degrees in electrical engineering from the Federal University of Itajubá (UNIFEI), Itajubá, Brazil, in 2001, 2004, and 2016, respectively.

From 2011 to 2022, he was with the Gnarus Institute, Itajubá. He is currently a Professor with UNIFEI. He has experience with the development of hardware and software for microcontrollers, DSPs, and FPGAs. His research interests include condition-based maintenance, frequency response analysis of electric machinery, power electronics, and control systems.

Dr. Sant'Ana is a member of Brazilian Power Electronics Society (SOBRAEP).

Coordenação de Aperfeiçoamento de Pessoal de Nível Superior (CAPES) - ROR identifier: 00x0ma614